

# Data-Driven Switch Fault Diagnosis for DC/DC Boost Converters in Photovoltaic Applications

Diego Rivelino Espinoza-Trejo , Senior Member, IEEE, Luis Miguel Castro , Ernesto Bárcenas , and José Pecina Sánchez , Member, IEEE

**Abstract**—Switch semiconductors are essential components in power electronics stages for photovoltaic (PV) systems, which are prone to failures caused mainly by thermal stress, thereby affecting PV energy production. Specifically, dc/dc boost power converters are commonly used as maximum power point tracking (MPPT) systems. Several works have been reported so far in the literature for switch fault detection and isolation (FDI) purposes in boost power converters. However, most of them require additional sensors and circuitry to those included in any PV system, which generate extra costs on the overall system. Hence, this work presents an efficient and low-cost switch fault diagnosis proposal, which requires only the most common measurements in PV systems, namely, PV current and voltage. This work departs from a data-driven FDI methodology for diagnosing switch open- and short-circuit faults in dc/dc boost converters. The experimental results have been evaluated against sudden irradiance changes and switch faults in a test bench of 350 W operating under a closed-loop nonlinear control action for MPPT purposes by using the dSpace 1104 board.

**Index Terms**—Multiclass classifiers, open-circuit faults, photovoltaic systems, short-circuit faults.

## I. INTRODUCTION

**A** HIGH penetration of photovoltaic (PV) generation into electrical grids demands high reliability standards such as security and predictability. PV generation operates mainly through different power electronics systems, basically made up by switch semiconductors, which are the most failure-prone elements mainly due to thermal stress [1]. Switch failures are broadly categorized as: 1) open-circuit faults (OCF); 2) short-circuit faults (SCF); and 3) intermittent gate-misfiring faults [2], which can seriously affect the power conversion system if any action is taken after fault triggering. Therefore, fault-tolerant

Manuscript received 9 October 2022; revised 24 January 2023 and 21 February 2023; accepted 16 March 2023. Date of publication 3 April 2023; date of current version 16 August 2023. (Corresponding author: Diego Rivelino Espinoza-Trejo.)

Diego Rivelino Espinoza-Trejo, Ernesto Bárcenas, and José Pecina Sánchez are with the Coordinación Académica Región Altiplano, Universidad Autónoma de San Luis Potosí, Matehuala, San Luis Potosí 78722, Mexico (e-mail: drespinozat@ieee.org; ernesto.barcenas@uaslp.mx; angel.pecina@uaslp.mx).

Luis Miguel Castro is with the Departamento de Energía Eléctrica, Universidad Nacional Autónoma de México, Coyoacan, Distrito Federal 04510, Mexico (e-mail: luismcastro@fi-b.unam.mx).

Color versions of one or more figures in this article are available at <https://doi.org/10.1109/TIE.2023.3262888>.

Digital Object Identifier 10.1109/TIE.2023.3262888

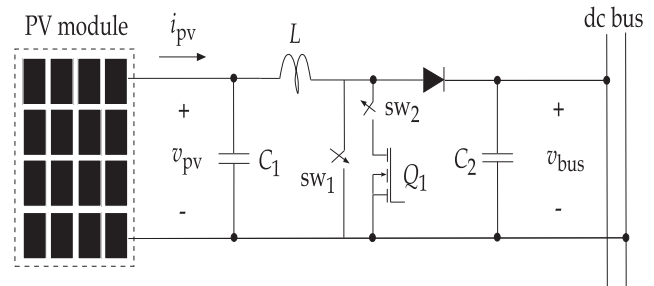


Fig. 1. DC/DC boost converter as interface between PV module and load.

design is proposed as one of the most important actions for improving the reliability of power electronics components [3]. As a consequence, sophisticated monitoring and fault detection and isolation (FDI) techniques are becoming mandatory for PV systems [4]. Particularly, the PV application presented in Fig. 1 is considered in this study, which has been employed for transformerless grid-connected PV configurations [5], power optimizers [6], [7], [8], and has been widely studied in the literature due to its attractive features that make it suitable for many other applications [9]. Nevertheless, the ideas exposed here could be extended to other PV configurations and will be explored in future works.

For the present study, a switch failure is not considered as a destructive event, as the PV module behaves as a current source (see Fig. 1). However, note that under switch fault scenarios, PV power drops to zero, thereby affecting energy production. In addition, the return on investment can be increased due to a long time for warranty replacement, and the forecasting PV production will also be affected by this kind of failure events. Consequently, several works have been reported in the literature to detect and isolate switch failures, which are briefly detailed in the next section.

## A. Literature Review

In [10], an FDI scheme was proposed for a quadratic boost converter. Switch and diode OCF and SCF can be diagnosed with this proposal. In this case, inductor voltages were selected as fault diagnosis characteristics, which implies adding an auxiliary winding to the magnetic core of the inductor for the voltage measurement. In addition, the PWM signal and a logic circuit are required for FDI purposes. Several OCF and SCF fault

diagnosis schemes have been proposed for single-switch dc/dc converters [11], [12], [13], [14]. In [11], the PWM signal and the inductor current were required for FDI purposes. In this case, switch faults can be detected and isolated in less than two switching periods. In [12], the inductor current, the input and output voltages of the boost converter were required for predicting the inductor current. Consequently, the error between the measured inductor current and its prediction was used to detect and isolate switch faults in less than one switching cycle. However, this proposal can be affected by parametric uncertainty, as threshold selection depends on converter's parameters. In [13], switch and diode OCF and SCF could be diagnosed in less than one switching cycle. For this, the diode voltage and a logic circuit must be added to the dc/dc converter. A comprehensive monitoring system was proposed in [14]. In this case, switch and diode OCF and SCF, switch and capacitor aging, and interturn fault of the inductor can be detected by using two electrical sensors and two temperature sensors. In [15], a fast switch fault diagnosis method was proposed for single- and dual-switch converters. For this, the magnetic component voltage and the gate driver signal of the dc/dc converter were required for diagnosing OCF and SCF. In [16], once more, the inductor current derivative and the gate driver signal were required for switch fault diagnosis and capacitor lifetime monitoring in nonisolated single-switch dc/dc converters. Here, a similar fault detection scheme to that given in [15] was proposed for switch fault diagnosis. However, in [16], a Rogowski coil sensor was proposed for estimating the inductor current derivative instead of an auxiliary winding, as suggested in [15]. Similarly, in [17], switch OCF and SCF diagnosis and fault-tolerant operation were proposed for boost dc/dc converters in PV applications. In this case, the switching command signal and the sign of the inductor current slope were required for fault detection and identification. Here, the maximum detection time was one switching period. On the other hand, a switch open-circuit fault detection and fault compensation schemes were proposed for a modified boost dc/dc converter for alternative energy harvesting systems in [18]. For switch OCF detection, an index was created by using the inductor and load currents and the inductor current reference of the closed-loop control structure, which makes the fault detection scheme dependent of control parameters. A model-based FDI approach was proposed in [19] for OCF and SCF in dc/dc boost converters. In this article, switch faults were modeled by using an additive structure. Here, a Luenberger observer was employed for fault identification purposes. For this, three measurements (PV current and voltage, output voltage) and the control signal were required for decoupling the residual signal from irradiance changes and load variations. The sign of the residual signal (positive or negative) was used for fault isolation purposes, while fault detection was achieved in eight switching periods. A similar work was proposed in [20], but in this case, a robust FDI scheme was achieved by using a high-gain observer by taking advantage of the integral action's effect of the nominal control after fault is triggered. For this, OCF and SCF were described as ever-growing signals, thereby enabling the suggested FDI scheme. More recently, a data-driven fault detection method was suggested in [21], which proposes to detect anomalies for any kind of dc/dc converter. Specifically, a statistical feature estimation using Gaussian process regression

is employed with fault detection objectives. In this context, training modeling implies to collect samples in real scenarios to detect anomalies adequately for each dc/dc converter. This in turn requires fault detection parameters adjustment for each application, which makes it an attractive but more complex methodology.

On the other hand, a short-circuit protection scheme with fault tolerance was proposed for boost switching dc/dc converters in [22]. Output short-to-ground and switch short-circuit fault scenarios can be handled by this proposal. After fault detection, the fault-tolerant action isolates the converter from its power supply, achieved in  $5 \mu\text{s}$ . For this, an inductor voltage sensor and the PWM signal are required for fault diagnosis purposes. It is worth mentioning here that the most recent short-circuit protection schemes for silicon carbide (SiC) metal-oxide-semiconductor field-effect transistor (MOSFET) look for compensating the short circuit withstand capability (amount of time from the start of short-circuit fault until the device is completely damaged), which is smaller than for silicon (Si) insulated gate bipolar transistor (IGBT) [23]. Nevertheless, note that if the power supply of the dc/dc boost converter is a PV array, then there is no damage after short-circuit faults as the PV array behaves as a current source. Hence, for the PV configuration studied in this article, a fast short-circuit fault detection is not mandatory.

Lastly, regarding machine learning techniques for fault classification, the present work has been inspired by recent works reported in the literature [24], [25], [26], [27]. In these works, special attention has been paid to faults related to the dc side of the PV system. A comprehensive review of fault classification techniques for PV systems has been presented in [24]. In [25], a hierarchical classification method was suggested as fault monitoring method to detect and classify line-to-line and line-to-ground faults at the dc side of PV systems by using three classifiers, namely: 1) support vector machines (SVM); 2) naive Bayes; and 3) logistic regression. Meanwhile, potential-induced degradation and light and enhanced temperature induced degradation failures were automatically predicted by using the principal component analysis method in combination with a k-nearest neighbor classifier. On the other hand, an intelligent detection algorithm for dc arc-faults was presented in [27], which is based on both the optimized variational mode decomposition and SVM.

With this background in mind, a qualitative comparison of fault diagnosis techniques for dc/dc converters is presented in Table I. The main contributions of the present FDI scheme are as follows.

- 1) The proposed scheme only requires the PV voltage and current sensors for diagnosing open- and short-circuit faults.
- 2) DC bus short-circuit faults (pole-to-pole) can be also detected because their behavior is similar to switch short-circuit fault conditions.
- 3) The proposed FDI algorithm is effective against drastic irradiance changes and temperature variations.
- 4) As opposed to other data-driven FDI schemes, normal and faulty samples from real scenarios are not required for training modeling.

**TABLE I**  
COMPARATIVE TABLE OF FAULT DIAGNOSIS TECHNIQUES FOR DC/DC CONVERTERS

Reference	Detection time	Required signals	Required sensors	Extra circuitry	Type of faults	Topology
[10]	Less than one switching cycle	Drive signal and polarity of inductor voltage	Inductor voltages (two sensors)	Yes	Switch and diode OCF and SCF	Quadratic single-switch dc/dc converters
[11]	Less than two switching cycles	Drive signal and slope of the inductor current	Inductor current	Yes	Switch OCF and SCF	Single switch dc/dc converters
[12]	Less than one switching cycle	Drive signal and predicted inductor current	Inductor current, input and output voltages of converter	No	Switch OCF and SCF	Boost dc/dc converters
[13]	Less than one switching cycle	Drive signal $S(t)$ , $V_{th1}$ , $V_{th2}$ and $S_r$ (time delay unit for $S(t)$ )	Diode voltage	Yes	Switch and diode OCF and SCF	Buck, boost and buck-boost dc/dc converters
[14]	Less than one switching cycle	Drive signal $S(t)$ , $v_s$ , $V_{in}$ , $V_{th1} - V_{th4}$ and $S_r$ (time delay unit for $S(t)$ )	Diode and inductor voltages, inductor current, ambient and capacitor temperatures	Yes	Switch and diode OCF/SCF, switch aging, capacitor aging, and interturn fault of the inductor	Single switch dc/dc converters
[15]	One switching cycle	Drive signal $s_1$	Magnetic component voltage	Yes	Switch OCF and SCF	most PWM dc/dc converters
[16]	Less than one switching cycle	Gate driver signal	Rogowski coil sensor	Yes	Switch OCF and SCF	Single switch dc/dc converters
[17]	One switching cycle	Drive signal and the sign of the inductor current slope	Inductor current	Yes	Switch OCF and SCF	Single switch dc/dc converters
[18]	–	Inductor current command	Inductor and load currents	No	Switch OCF	Modified dc/dc boost converter
[19]	Eight switching cycles	Control signal	PV current and voltage, output voltage	No	Switch OCF and SCF	dc/dc boost converter
[20]	Eight switching cycles	Control signal	PV current and voltage, output voltage	No	Switch OCF and SCF	dc/dc boost converter
Present work	Five switching cycles	None	PV current and voltage	No	Switch OCF and SCF	dc/dc boost converter

Note: For [13],  $V_{th1}$  and  $V_{th2}$  are thresholds related to internal parameters of the dc/dc converter, and for [14],  $V_{th1}$ – $V_{th4}$  are thresholds related to internal parameters of the dc/dc converter,  $v_s$  represents switch voltage of the dc/dc converter, and  $V_{in}$  denotes input supply voltage.

In connection with the above contributions, this research work is justifiable from various fronts. The two employed sensors are the most common measurements in any PV system, which permits to achieve a cost-effective solution for the switch FDI problem. Equally important is the fact that this novel FDI scheme employs conventional PV cell models, which results in a much reduced complexity of the classification model training. All aspects considered, with this FDI proposal the reliability standards of security and predictability in PV systems are increased. Additionally, it is worth mentioning that data separability, as posed in this work, is considered as a novel idea for fault diagnosis purposes, which is detailed in the next section. Admittedly, the suggested FDI scheme depends on the power converter topology and is exclusive for PV applications. However, as mentioned earlier, this PV configuration is widely employed

in different configurations, for instance, in power optimizers. Consequently, the ideas exposed here will be explored in other PV configurations in the future.

The rest of this article is organized as follows. In Section II, data separability for open- and short-circuit faults is demonstrated by using conventional PV cell modeling. Next, the fault classification algorithm is presented in Section III. The experimental results are shown in Section IV. Finally, Section V concludes the article.

## II. DATA SEPARABILITY

The studied system in this article is presented in Fig. 1, which is constituted by a PV module (*or PV array*), a dc/dc boost converter, and the load element (dc bus). In Fig. 1, SCF is

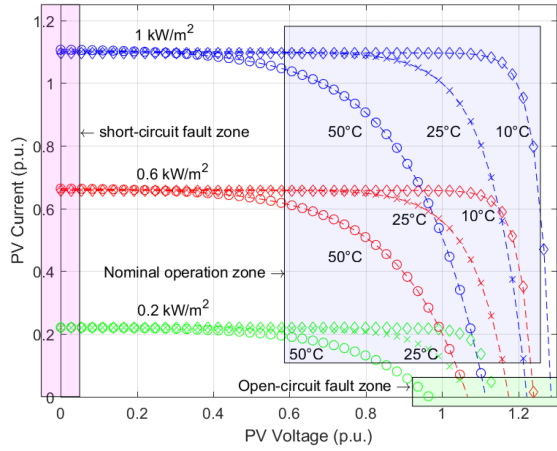


Fig. 2. Graphical representation of operating points under nominal and fault conditions for different irradiance and temperature levels.

represented by the normally open switch  $sw_1$ , while OCF is depicted by the normally closed switch  $sw_2$ .

Also,  $v_{pv}$  represents the input voltage in the terminals of the capacitor  $C_1$ , and  $i_{pv}$  denotes the PV current generated by the PV module. The dynamic modeling of this converter is presented in the Appendix A in (4), which is only used for the nominal control system design. However, it is worth highlighting that only  $(i_{pv}, v_{pv})$  are required for the proposed FDI scheme.

Under a SCF, ideally, the PV voltage goes down to zero and the PV current reaches the short circuit current value. Also, under an OCF, the PV current goes down to zero and the PV voltage increases to the open-circuit value. These fault conditions are illustrated in Fig. 2 for different irradiance and temperature levels (see OCF and SCF zones).

It is well known that irradiance changes mainly impact the PV current, while temperature variations impact the open-circuit voltage, which can also be observed in Fig. 2. As an example, note that the PV voltage is zero in the SCF zone. As a consequence, the PV operating point—after fault is triggered—mainly depends on the irradiance level. Note that the PV current and voltage in Fig. 2 are given in p.u. based on their rated current or voltage at the maximum power point under standard test conditions. In this way, the results presented in this article are valid for any PV module (or array) used as input power source for dc/dc boost converters. Moreover, it is worth mentioning that the characteristics curves in Fig. 2 were obtained by using the simplified model with one diode, [28], [29], which has also been used for model training. As a result, this switch FDI proposal does not require actual faulty conditions data for training purposes, which is considered as one of the main contributions of this work.

Three zones can be distinguished in Fig. 2, which are related to the nominal operation, SCF and OCF zones. The nominal operation zone can be modified as needed. In Fig. 2, it is defined by the most common operating conditions, i.e., PV module operation at the maximum power point (MPP). However, this zone can still be expanded, for example, to improve the robustness of the diagnostic scheme against disturbances caused by

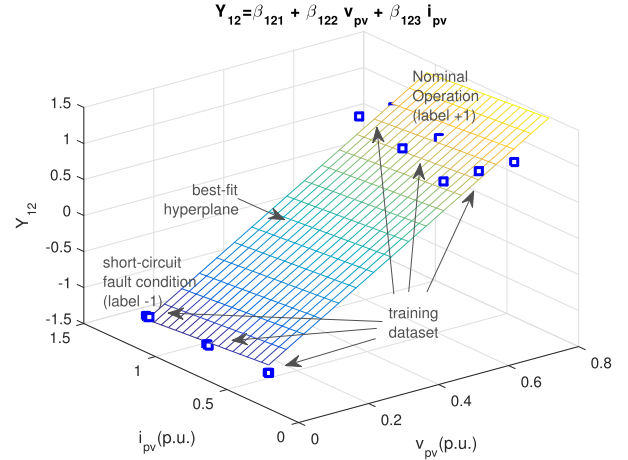


Fig. 3. Training dataset and best-fit hyperplane for short-circuit faults.

irradiance changes. OCF zone mainly depends on maximum and minimum temperature levels of the PV system's geographical location. Nevertheless, it is worth noting that temperature levels are also required for PV system's sizing. Consequently, there is no inconvenience for model training purposes. Meanwhile, the SCF zone is defined in a simpler way, as PV current mainly depends on the different irradiance levels, which can be known for any location. Thus, as visualized in Fig. 2, data separability can be guaranteed for almost any PV operating point in spite of irradiance and temperature variations. As a result, the switch FDI issue considered in this work can be solved by using multiclass classifiers, which is developed in the next section.

### III. FAULT DIAGNOSIS SYSTEM

The FDI scheme proposed in this article departs from a training dataset given by

$$x^{(1)}, x^{(2)}, \dots, x^{(M)}, \quad y_{ij}^{(1)}, y_{ij}^{(2)}, \dots, y_{ij}^{(M)},$$

where  $x$  is a vector whose components are PV voltage  $v_{pv}$  and current  $i_{pv}$ , i.e.,

$$x^{(k)} = \begin{bmatrix} v_{pv}^{(k)} \\ i_{pv}^{(k)} \end{bmatrix}^T, \quad \forall k \in \{1, \dots, M\}.$$

For this study, the dataset was obtained by using a PV cell model given in [28] and [29] by taking into account three different levels of irradiance and three temperature levels, which can be observed in Fig. 4. Besides,  $y_{ij}^{(k)}$  is the outcome, which takes only two values, i.e., if  $x^{(k)}$  belongs to class  $i$ , then  $y_{ij}^{(k)} = +1$ , and  $y_{ij}^{(k)} = -1$ , if  $x \in$  class  $j$ . Subscripts  $i, j \in \{1, 2, 3\}$  are associated with three classes defined as follows: 1) Nominal operation (N.O.); 2) Short-circuit fault (S.C.); and 3) Open-circuit fault (O.C.).

Hence, a three-class classifier is required for FDI purposes, which is built departing from three boolean classifiers. One-versus-one multiclass classifier methodology has been suggested for fault isolation purposes. The function  $\hat{y}_{ij}$  given in (1) is proposed as a boolean classifier for every pair of classes  $i$

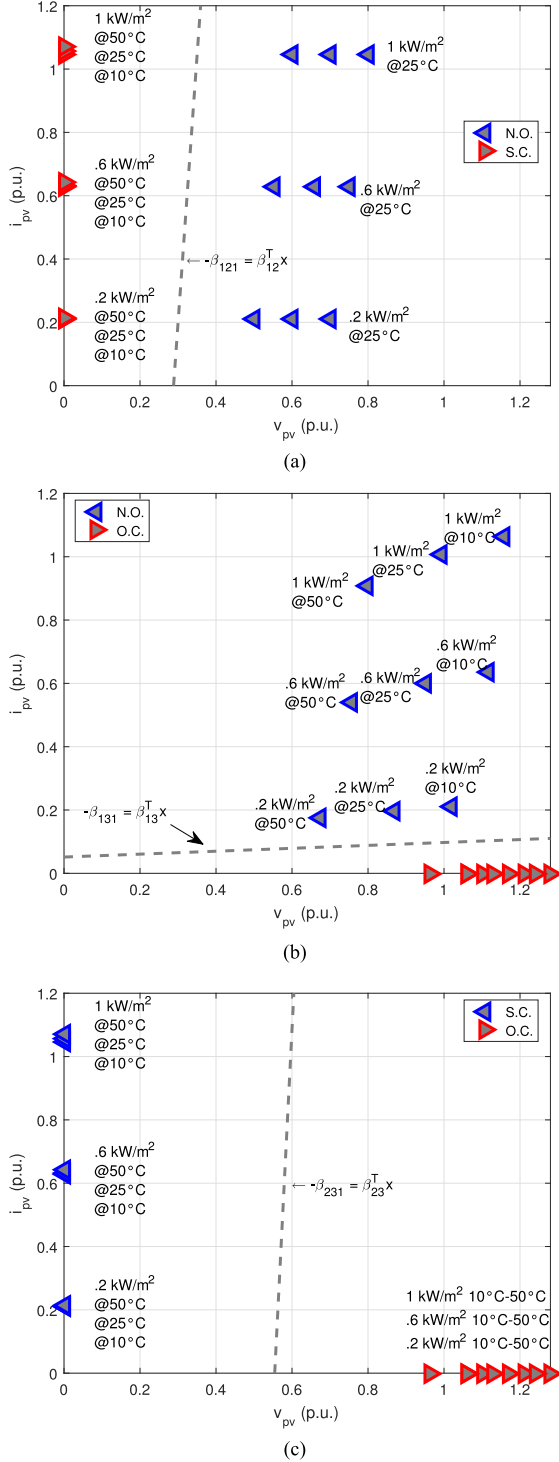


Fig. 4. Graphical representation of training dataset for fault classification: (a) 1 versus 2, (b) 1 versus 3, and (c) 2 versus 3.

and  $j, i < j$ , such that  $i, j \in \{1, 2, 3\}$

$$\hat{y}_{ij} = \text{sign}(Y_{ij}) \quad (1)$$

where the sign function argument is given by the linear regressor

$$Y_{ij} = \tilde{f}_{ij}(x) = \beta_{ij1} + \beta_{ij}^T \cdot x \quad (2)$$

TABLE II  
TRAINING DATASET FOR BOOLEAN CLASSIFIER FOR PAIR OF CLASSES 1 AND 2

Cond.	Irr.	Temp. ( $^{\circ}\text{C}$ )	$v_{pv}$ (p.u.)	$i_{pv}$ (p.u.)	$y_{12}$
N.O	1	25	0.8	1.046	+1
		25	0.7	1.046	+1
		25	0.6	1.046	+1
	0.6	25	0.75	0.6277	+1
		25	0.6588	0.6277	+1
		25	0.5534	0.6277	+1
	0.2	25	0.7	0.2092	+1
		25	0.6	0.2092	+1
		25	0.5007	0.2092	+1
S.C.	1	10	0	1.0462	-1
		25	0	1.0549	-1
		50	0	1.0695	-1
	0.6	10	0	0.6277	-1
		25	0	0.6329	-1
		50	0	0.6416	-1
	0.2	10	0	0.2092	-1
		25	0	0.2109	-1
		50	0	0.2138	-1

Note: Units for irradiance (Irr.) column are given in  $\text{kW/m}^2$ .

TABLE III  
REGRESSORS PARAMETERS

Parameter	Value	Parameter	Value	Parameter	Value
$\beta_{121}$	-0.8548	$\beta_{122}$	2.9648	$\beta_{123}$	-0.1758
$\beta_{131}$	-0.4950	$\beta_{132}$	-0.4431	$\beta_{133}$	9.6293
$\beta_{231}$	0.9414	$\beta_{232}$	-1.6980	$\beta_{233}$	0.0712

where  $\beta_{ij} = [\beta_{ij2}, \beta_{ij3}]^T$  and  $x = [v_{pv}, i_{pv}]^T$ . The linear regressor is trained such that

$$\tilde{f}_{ij} : x \in \mathbb{R}^2 \rightarrow \{+1, -1\}.$$

As example, the regressor  $Y_{12} = \tilde{f}_{12}(x)$  is trained by using the training dataset given in Table II. Numerical values for  $v_{pv}, i_{pv}$  in Table II were obtained using a conventional PV cell model [28], considering the irradiance and temperatures values shown in Table II. Note that PV voltage and current are given in p.u. units, and the outcome  $y_{12}$  is given by the labels +1 and -1. In addition, data are organized by considering the classes 1 (N.O.) and 2 (S.C.) and the different levels of irradiance and temperature.

Thus, for every pair of classes  $i$  and  $j, i < j$ , the value  $Y_{ij} = \tilde{f}_{ij}(x)$  is a number which is near +1 when  $y_{ij}^{(k)} = +1$ , and near -1 when  $y_{ij}^{(k)} = -1$ . Regressor parameters  $\beta_{ij1}, \beta_{ij2}, \beta_{ij3}$  are chosen to minimize the sum squared error [30]

$$\left(y_{ij}^{(1)} - \tilde{f}_{ij}(x^{(1)})\right)^2 + \dots + \left(y_{ij}^{(M)} - \tilde{f}_{ij}(x^{(M)})\right)^2. \quad (3)$$

Specifically, the best-fit hyperplane (minimizing the sum squared error) for boolean classifier  $\hat{y}_{12}$  is shown in Fig. 3, with training data given in Table II are also illustrated in this figure. The hyperplane illustrated in Fig. 3 was obtained by using the parameters  $\beta_{121}, \beta_{122}, \beta_{123}$  shown in Table III. A brief description of how parameters  $\beta$  for classifier  $Y_{12}$  are obtained is presented

in Appendix B. A similar procedure can be carried out for the other two regressors, i.e.,  $Y_{13}$  and  $Y_{23}$ .

Consequently

$$\hat{y}_{ij} = \begin{cases} 1 & \text{if } y_{ij} \in \text{Class } i, \\ -1 & \text{if } y_{ij} \in \text{Class } j. \end{cases}$$

Hence, given a feature vector  $x$ ,  $\hat{y}_{ij}$  is the prediction of the  $i$  vs  $j$  classifier, with  $\hat{y}_{ij} = 1$  meaning that the one-vs.-one classifier is guessing that  $y_{ij} = i$ . Therefore,  $\hat{y}_{ij} = 1$  is considered as one vote for class  $i$ , and  $\hat{y}_{ij} = -1$  as one vote for class  $j$ . Thus, the final estimated class is obtained by majority voting [30]. In general terms, there are  $K(K-1)/2$  such pairs of classifiers, where  $K$  is the number of classes. Thus, in this study there are three boolean classifiers, namely,  $\hat{y}_{12}$ ,  $\hat{y}_{13}$ , and  $\hat{y}_{23}$ . The decision boundary for boolean classifier  $\hat{y}_{12}$  proposed in this work is shown in Fig. 4(a), which is obtained by setting  $Y_{12} = 0$  in (2), such that  $-\beta_{123} = \beta_{12}^\top x$ . Note that it is able to adequately distinguish a SCF from a nominal operation for any irradiance and temperature conditions.

On the other hand, the decision boundary of classifier for classes 1 versus 3 is shown in Fig. 4(b). It must be able to classify an open-circuit fault and a nominal condition adequately. As shown in Fig. 4(b), data separability could be compromised for irradiance levels lower than  $200 \text{ W/m}^2$ . Nevertheless, PV systems shut down at a minimum irradiance level such that it is not mandatory to operate the FDI algorithm for very low irradiance levels. As a consequence, this classifier will satisfactorily operate for most temperature and irradiance conditions. It is worth mentioning that this classifier was trained by taking into account only data of the worst case of irradiance level ( $200 \text{ W/m}^2$ ) for the N.O. class. Lastly, the decision boundary of classifier for classes 2 versus 3 is illustrated in Fig. 4. As shown in this figure, it satisfactorily distinguishes short- and open-circuit faults for any irradiance and temperature conditions.

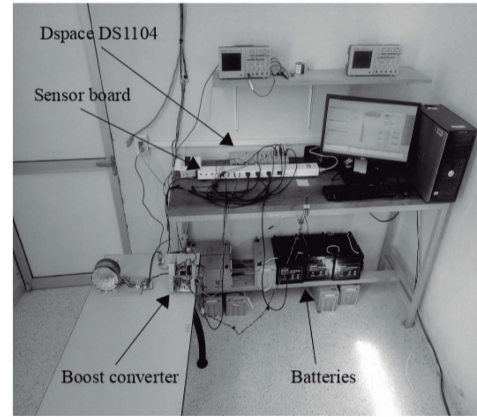
*Remark 1:* More sophisticated techniques are available for fault classification (FC), for instance, logistic regression, support vector machines, neural networks, [24], [25], [26], [27], which will be explored in future works. However, the proposed FDI scheme departs from a simple, but effective data-driven perspective by using basic machine learning tools.

#### IV. EXPERIMENTAL RESULTS

Experimental validation of the FDI algorithm proposed in this article is given in this section. For this, a dc/dc boost converter rated at  $350 \text{ W}$  and operating at a switching frequency  $f_{sw} = 10 \text{ kHz}$ , 5 batteries in series-connection as load ( $12 \text{ V}$   $80 \text{ Ah}$  each), and two PV modules of  $175 \text{ W}$  each in parallel-connection were integrated in the prototype, as illustrated in Fig. 5. In these results, the irradiance changes were emulated by disconnecting (for irradiance drop emulation) one of the two PV modules through a mechanical switch. The parameters of this power converter are given as follows:  $L = 1.2 \text{ mH}$ ,  $C_1 = 30 \text{ }\mu\text{F}$  and  $C_2 = 94 \text{ }\mu\text{F}$ . The MOSFET used in this prototype was IRFP250 N and the diode was STTH30RD4W. In this case, the dc/dc boost converter is operating under the influence of a closed-loop control action [8], which is briefly described in



(a)



(b)

Fig. 5. PV Test Bench. (a) PV modules. (b) Prototype of boost DC/DC converter.

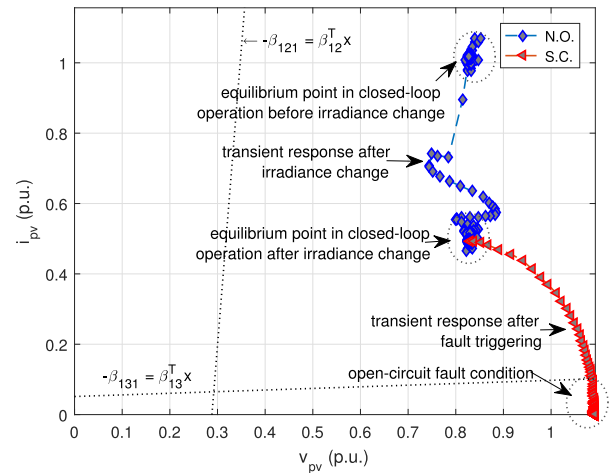


Fig. 6. Transient and steady-state responses illustrated in plane V-I for irradiance change and open-circuit fault conditions.

Appendix A. Here, settling time was selected as  $t_s = N \times T_{sw}$ , where  $T_{sw} = 1/f_{sw}$  is the switching period and  $N$  is an integer. The dSpace 1104 board has been considered for data acquisition and controller implementation by using a sampling frequency of  $40 \text{ kHz}$ . A downsampling factor of  $N_{ds} = 5$  has been used merely for the purpose of reducing the computational burden of the dSpace board aiming at facilitating the virtual interface

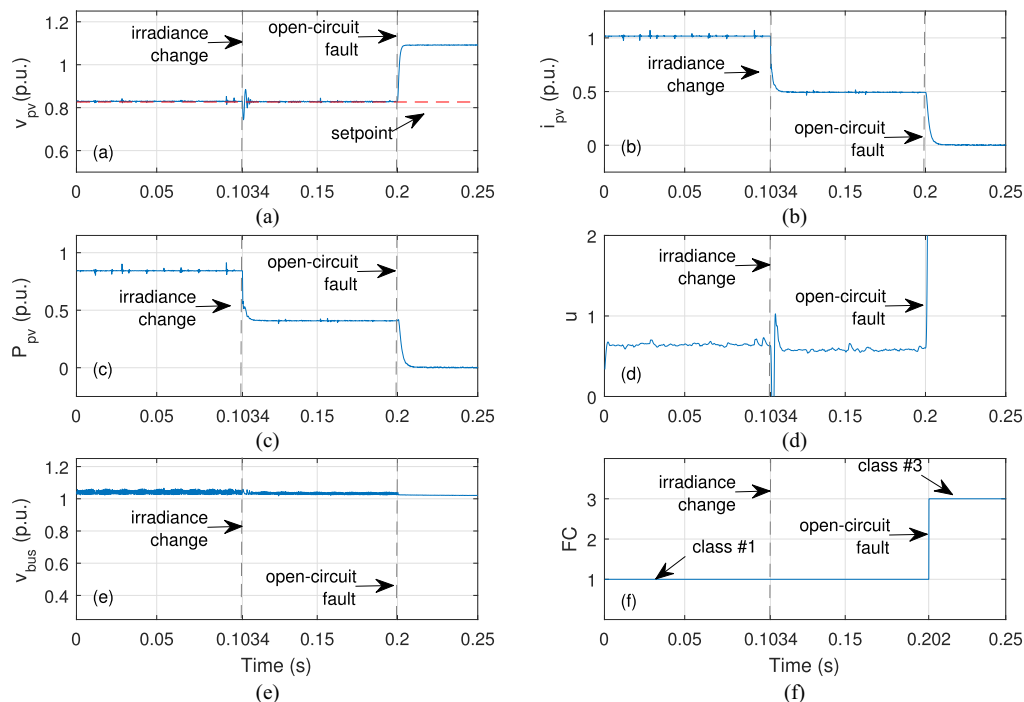


Fig. 7. Experimental results (open-circuit fault): (a) PV voltage  $v_{pv}$  in p.u., (b) PV current  $i_{pv}$  in p.u., (c) PV power  $P_{pv}$  in p.u., (d) control action  $u$ , (e) output voltage  $v_{bus}$  in p.u., and (f) fault classification signal FC.

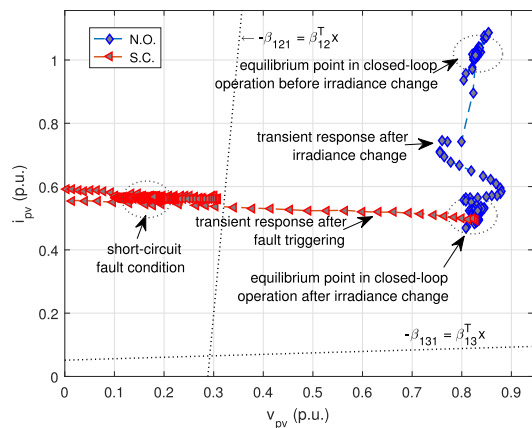


Fig. 8. Transient and steady-state responses illustrated in plane V-I for irradiance change and short-circuit fault conditions.

tasks during the experiments. However, this is not mandatory for the proposed FDI scheme. Consequently, with an evaluation window of 0.25 s, a testing dataset with 2000 samples has been used for each of the two experiments presented in this section. The experimental results are presented in Figs. 6–9. All variables illustrated in these figures are expressed in p.u. values based on their rated values, defined in Table IV, where  $P_{pv}$  is the PV power and  $v_{bus}$  is the output voltage of the dc/dc boost converter.

### A. Open-Circuit Fault Scenario

The open-circuit fault scenario is described in Figs. 6 and 7. First, a sudden irradiance drop is induced about  $t = 0.1034$  s, which can be observed through the PV current in Fig. 7(b).

TABLE IV

RATED VALUES FOR THE EXPERIMENTAL RESULTS

Variable	Rated value	Variable	Rated value
$v_{pv}$	36.3 (V)	$i_{pv}$	9.64 (A)
$P_{pv}$	350 (W)	$v_{bus}$	60 (V)

In addition, this change can be identified in the PV power, as illustrated in Fig. 7(c). A transient response is also perceived in the PV voltage because of this irradiance change. Here, the control action  $u$  compensates this disturbance by guaranteeing PV voltage regulation at the voltage reference given by  $v_{pv}^* = 0.82$  p.u., as shown in Fig. 7(a). Nevertheless, the fault classification FC signal shows class number 1 as result, i.e., it is not affected by this disturbance, as observed in Fig. 7(f). Next, an open-circuit fault occurs at  $t = 0.2$  s. As a consequence, the PV current and power fall to zero [see Fig. 7(b) and (c)]. Also, the control signal  $u$  (duty cycle) tries to compensate the failure event. However, it diverges due to the integral control action of the proportional-integral-derivative (PID) controller. Thus, the FC signal is triggered and associated with class number 3. In this case, the fault isolation time is 2 ms, [see Fig. 7(f)] which corresponds to 16 sampling periods (four switching cycles).

In addition, transient and steady-state responses for the open-circuit fault scenario are illustrated in Fig. 6 in the plane V-I. First, a closed-loop equilibrium point is observed before the irradiance change. Here, the PV current and voltage are at their maximum value  $i_{pv} = 1$  p.u. and  $v_{pv} = 0.82$  p.u., approximately. Next, after the transient response associated with the sudden irradiance drop of 50%, a new closed-loop equilibrium

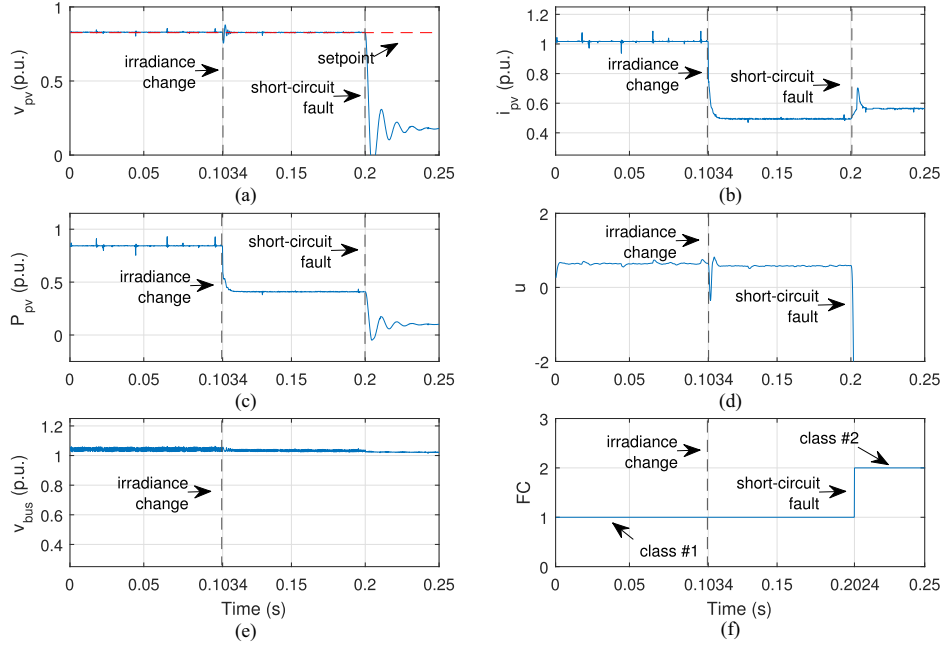


Fig. 9. Experimental results (short-circuit fault): (a) PV voltage  $v_{pv}$  in p.u., (b) PV current  $i_{pv}$  in p.u., (c) PV power  $P_{pv}$  in p.u., (d) control action  $u$ , (e) output voltage  $v_{bus}$  in p.u., and (f) fault classification signal FC.

point is reached at  $i_{pv} = 0.5$  p.u. and  $v_{pv} = 0.82$  p.u. After this, the transient and steady-state responses associated with the open-circuit fault can be observed in the figure together with the decision boundaries for classifiers  $\hat{y}_{13}$  and  $\hat{y}_{12}$  (straight lines). Therefore, it can be concluded that transient responses do not affect the open-circuit fault detection.

### B. Short-Circuit Fault Scenario

The short-circuit fault scenario is now described in Figs. 8 and 9. Again, at  $t = 0.1034$  s there is a sudden irradiance drop, which can be observed through the PV current and power in Fig. 9(b) and (c). Although, the FC signal is kept in class 1, as shown in Fig. 9(f). After this, at  $t = 0.2$  s there is a short-circuit fault. Here, the PV current increases to its short-circuit value, [see Fig. 9(b)]. While, PV voltage and PV power fall almost to zero, [see Fig. 9(a) and (c)]. It is due to an internal resistance into the inductor. The control signal once more diverges due to the integral control action in the PID controller, as can be observed in Fig. 9(d). However, the FC signal indicates class number 2, as shown in Fig. 9(f). Once more, the transient and steady-state responses are shown in Fig. 8. Three equilibrium points are visualized in Fig. 8. One of them is related to the short-circuit fault condition, while the other two correspond to closed-loop nominal operation. In addition, transient responses associated with irradiance change and short-circuit fault can also be observed in the same graph together with the decision boundaries. In this case, the fault isolation time is 2.4 ms [see Fig. 9(f)], which implies 20 sampling periods (five switching cycles), approximately. Consequently, through this experimental validation, the FDI proposal has been rigorously validated through real scenarios by taking into account irradiance changes and switch OCF and SCF.

## V. CONCLUSION

PV systems are being increasingly integrated into the electrical grids, which implies that PV generation must be reliable and predictable. Consequently, fault-tolerant control structures are becoming more important for this kind of systems. For this, FDI algorithms are mandatory for fault decision-making. In this way, this article proposed a new switch open- and short-circuit FDI algorithm by using only two sensors for dc/dc boost converters, which are commonly employed for PV MPPT applications. This FDI proposal has been evaluated against switch faults and irradiance changes by obtaining satisfactory results. This same idea could be extrapolated to power optimizers by using the same dc/dc converter topology employed in this work. As future work, data-driven FDI techniques will be reviewed for other and more complex PV configurations. Note that only two sensors are required for fault classification purposes, which is one of the contributions of this work in comparison with previous works, which require extra sensors and circuitry. Also, it is worth mentioning that PV voltage and current are the most common measurements in any PV system for MPP tracking (MPPT) algorithms. Hence, the FDI scheme proposed in this work is considered as a noninvasive and economically attractive FDI scheme, which could be easily integrated to the most recent monitoring systems.

## APPENDIX A NOMINAL CONTROLLER DERIVATION

The nominal controller is developed in this section. Departing from Fig. 1, the following averaged model is obtained:

$$\begin{aligned} C_1 \dot{x}_1 &= -x_2 + i_{pv} \\ L \dot{x}_2 &= x_1 - x_3 + x_3 u \end{aligned}$$

$$C_2 \dot{x}_3 = x_2 - i_o - x_2 u \quad (4)$$

where the state vector is defined by  $x = (x_1, x_2, x_3)^T = (v_{pv}, i_L, v_{bus})^T$ . As can be observed from Fig. 1,  $v_{pv}$  represents the input voltage in the terminals of the capacitor  $C_1$ ,  $i_L$  the current of inductor  $L$ , and  $v_{bus}$  the voltage in the terminals of the output capacitor  $C_2$ . Also,  $i_{pv}$  in (4) denotes the PV current generated by the PV module,  $i_o$  the load current and  $u$  the control variable (duty cycle for the switch  $Q_1$ , see Fig. 1), which has a limited operating range,  $u \in [0, 1]$ . The state feedback control law given by

$$u = \left(1 - \frac{x_1}{x_3}\right) - \frac{LC_1}{x_3} v \quad (5)$$

reduces the input–output mapping to

$$\ddot{y} = v + \frac{1}{C_1} d(i_{pv}) \quad (6)$$

where  $v$  is constructed departing from a PID controller

$$v = K_p e + K_d \frac{de}{dt} + K_i \int edt + \ddot{y}^* \quad (7)$$

where  $e = y^* - y$  with  $y^* = x_1^*$ . Hence,  $y^*$  is selected to guarantee the MPP in the PV module. The PID controller gains ( $K_p$ ,  $K_i$ ,  $K_d$ ) are defined to achieve a desired step response. Hence, the PID controller gains are chosen as  $K_d = 4f_{sw} N^{-1}(p+2)$ ,  $K_p = 16f_{sw}^2 N^{-2} \xi^{-2}(2p\xi^2 + 1)$ ,  $K_i = 64f_{sw}^3 N^{-3} \xi^{-2} p$ , where  $f_{sw}$  is the switching frequency,  $\xi$  is the damping factor,  $p \in \mathbb{R}^+$  and the settling time is chosen as  $t_s = N \times T_{sw}$ , where  $N$  is an integer and  $T_{sw} = 1/f_{sw}$ , [31], [32]. In this way, departing from (7), the auxiliary control law  $v$  results as

$$v = K_p e + K_i \int edt + \frac{K_d}{C_1} (x_2 - i_{pv}). \quad (8)$$

## APPENDIX B

### REGRESSOR'S PARAMETERS DERIVATION

Derivation of the set of parameters  $\beta$  for the classifier  $Y_{12}$  is presented in this section. However, a similar procedure can be carried out for the other two Boolean classifiers, namely,  $Y_{13}$  and  $Y_{23}$ . For this, equation given in (2) can be written in matrix form for the classifier  $Y_{12}$  as  $Y = AX$ , with

$$Y = [Y_{12}^{(1)}, \dots, Y_{12}^{(M)}]^T \in \mathbb{R}^{M \times 1},$$

$$X = [\beta_{121}, \beta_{122}, \beta_{123}]^T \in \mathbb{R}^{3 \times 1}$$

and

$$A = \begin{bmatrix} 1 & v_{pv}^{(1)} & i_{pv}^{(1)} \\ \vdots & \vdots & \vdots \\ 1 & v_{pv}^{(M)} & i_{pv}^{(M)} \end{bmatrix} \in \mathbb{R}^{M \times 3}$$

where  $M$  is the number of samples used for training. Note that parameters  $\beta$  are included in the solution vector  $X$ . However, for most cases this equation has no solution. But, it is well known that the optimal solution  $\hat{X}$  of this matrix equation can be found with the pseudoinverse of matrix  $A$ , i.e.,  $\hat{X} =$

$A^\dagger Y = (A^T A)^{-1} A^T Y$ ; as it turns out, it can be demonstrated that this solution minimizes the sum squared error  $\epsilon$  in (3), i.e.,  $\|Y - A\hat{X}\|^2 = \|\epsilon\|^2$ . Hence, for the selection of parameters  $\beta$ , we have used the dataset given in Table II and the command *regress* in MATLAB, which requires vector  $Y$  and matrix  $A$  as inputs, which are obtained through the data training process.

## REFERENCES

- [1] F. Chan and H. Calleja, "Reliability estimation of three single-phase topologies in grid-connected PV systems," *IEEE Trans. Ind. Electron.*, vol. 58, no. 7, pp. 2683–2689, Jul. 2011, doi: [10.1109/TIE.2010.2060459](https://doi.org/10.1109/TIE.2010.2060459).
- [2] B. Lu and S. K. Sharma, "A literature review of IGBT fault diagnostic and protection methods for power inverters," *IEEE Trans. Ind. Appl.*, vol. 45, no. 5, pp. 1770–1777, Sep./Oct. 2009, doi: [10.1109/TIA.2009.2027535](https://doi.org/10.1109/TIA.2009.2027535).
- [3] H. Wang, M. Liserre, and F. Blaabjerg, "Toward reliable power electronics: Challenges, design tools, and opportunities," *IEEE Ind. Electron. Mag.*, vol. 7, no. 2, pp. 17–26, Jun. 2013, doi: [10.1109/MIE.2013.2252958](https://doi.org/10.1109/MIE.2013.2252958).
- [4] G. Di Lorenzo, R. Araneo, M. Mitolo, A. Niccolai, and F. Grimaccia, "Review of O&M Practices in PV plants: Failures, solutions, remote control, and monitoring tools," *IEEE J. Photovolt.*, vol. 10, no. 4, pp. 914–926, Jul. 2020, doi: [10.1109/JPHOTOV.2020.2994531](https://doi.org/10.1109/JPHOTOV.2020.2994531).
- [5] N. Vazquez, J. Vazquez, Joaquín Vaquero, C. Hernandez, E. Vazquez, and René Osorio, "Integrating two stages as a common-mode transformerless photovoltaic converter," *IEEE Trans. Ind. Electron.*, vol. 64, no. 9, pp. 7498–7507, Sep. 2017, doi: [10.1109/TIE.2017.2682014](https://doi.org/10.1109/TIE.2017.2682014).
- [6] G. R. Walker and P. C. Sernia, "Cascaded DCDC converter connection of photovoltaic modules," *IEEE Trans. Power Electron.*, vol. 19, no. 4, pp. 1130–1139, Jul. 2004, doi: [10.1109/TPEL.2004.830090](https://doi.org/10.1109/TPEL.2004.830090).
- [7] A. I. Bratcu, I. Munteanu, S. Bacha, D. Picault, and B. Raison, "Cascaded DC–DC converter photovoltaic systems: Power optimization issues," *IEEE Trans. Ind. Electron.*, vol. 58, no. 2, pp. 403–411, Feb. 2011, doi: [10.1109/TIE.2010.2043041](https://doi.org/10.1109/TIE.2010.2043041).
- [8] D. R. Espinoza Trejo, S. Taheri, J. L. Saavedra, P. Vázquez, C. H. De Angelo, and José A. Pecina-Sánchez, "Nonlinear control and internal stability analysis of series-connected boost DC/DC converters in PV systems with distributed MPPT," *IEEE J. Photovolt.*, vol. 11, no. 2, pp. 504–512, Mar. 2021, doi: [10.1109/JPHOTOV.2020.3041237](https://doi.org/10.1109/JPHOTOV.2020.3041237).
- [9] M. Forouzes, Y. P. Siwakoti, S. A. Gorji, F. Blaabjerg, and B. Lehman, "Step-up DC–DC converters: A comprehensive review of voltage-boosting techniques, topologies, and applications," *IEEE Trans. Power Electron.*, vol. 32, no. 12, pp. 9143–9178, Dec. 2017, doi: [10.1109/TPEL.2017.2652318](https://doi.org/10.1109/TPEL.2017.2652318).
- [10] L. Chen, X. Zhao, and S. X. Tang, "Online fault diagnosis method for high-performance converters using inductor voltage polar signatures," *IEEE Access*, vol. 8, pp. 179778–179788, 2020, doi: [10.1109/ACCESS.2020.3024549](https://doi.org/10.1109/ACCESS.2020.3024549).
- [11] E. Jamshidpour, P. Poure, E. Gholipour, and S. Saadate, "Single-switch DC–DC converter with fault-tolerant capability under open- and short-circuit switch failures," *IEEE Trans. Power Electron.*, vol. 30, no. 5, pp. 2703–2712, May 2015, doi: [10.1109/ACCESS.2020.3024549](https://doi.org/10.1109/ACCESS.2020.3024549).
- [12] E. Pazouki, Y. Sozer, and J. A. De Abreu-García, "Fault diagnosis and fault-tolerant control operation of nonisolated DC–DC converters," *IEEE Trans. Ind. Appl.*, vol. 54, No 1, pp. 310–320, Jan./Feb. 2018, doi: [10.1109/TIA.2017.2751547](https://doi.org/10.1109/TIA.2017.2751547).
- [13] H. Givi, E. Farjah, and T. Ghanbari, "Switch and diode fault diagnosis in nonisolated DC–DC converters using diode voltage signature," *IEEE Trans. Ind. Electron.*, vol. 65, No 2, pp. 1606–1615, Feb. 2018, doi: [10.1109/TIE.2017.2733486](https://doi.org/10.1109/TIE.2017.2733486).
- [14] H. Givi, E. Farjah, and T. Ghanbari, "A comprehensive monitoring system for online fault diagnosis and aging detection of non-isolated DC-DC converters' components," *IEEE Trans. Power Electron.*, vol. 34, no. 7, pp. 6858–6875, Jul. 2019, doi: [10.1109/TPEL.2018.2875830](https://doi.org/10.1109/TPEL.2018.2875830).
- [15] S. Nie, X. Pei, Y. Chen, and Y. Kang, "Fault diagnosis of PWM DC-DC converters based on magnetic component voltages equation," *IEEE Trans. Power Electron.*, vol. 29, no. 9, pp. 4978–4988, Sep. 2014, doi: [10.1109/TPEL.2013.2283881](https://doi.org/10.1109/TPEL.2013.2283881).
- [16] E. Farjah, H. Givi, and T. Ghanbari, "Application of an efficient rogowski coil sensor for switch fault diagnosis and capacitor ESR monitoring in nonisolated single-switch DC-DC converters," *IEEE Trans. Power Electron.*, vol. 32, no. 2, pp. 1442–1456, Feb. 2017, doi: [10.1109/TPEL.2016.2552039](https://doi.org/10.1109/TPEL.2016.2552039).

- [17] E. Jamshidpour, P. Poure, and S. Saadate, "Photovoltaic systems reliability improvement by real-time FPGA-Based switch failure diagnosis and fault-tolerant DC-DC converter," *IEEE Trans. Ind. Electron.*, vol. 62, no. 11, pp. 7247–7255, Nov. 2015, doi: [10.1109/TIE.2015.2421880](https://doi.org/10.1109/TIE.2015.2421880).
- [18] T. Kim, H. W. Lee, and S. Kwak, "Open-circuit switch-fault tolerant control of a modified boost DC-DC converter for alternative energy systems," *IEEE Access*, vol. 7, pp. 69535–69544, 2019, doi: [10.1109/ACCESS.2019.2919238](https://doi.org/10.1109/ACCESS.2019.2919238).
- [19] D. R. Espinoza-Trejo, E. Bárcenas, J. E. Hernández-Díez, G. Bossio, and G. Espinosa-Pérez, "Open- and short-circuit fault identification for a boost dc/dc converter in PV MPPT systems," *Energies*, vol. 11, no. 3, pp. 1–15, 2018, doi: [10.3390/en11030616](https://doi.org/10.3390/en11030616).
- [20] D. R. Espinoza Trejo, S. Taheri, and J. A. Pecina Sánchez, "Switch fault diagnosis for boost DC-DC converters in photovoltaic MPPT systems by using high-gain observers," *IET Power Electron.*, vol. 12, no. 11, pp. 2793–2801, 2019, doi: [10.1049/iet-pel.2018.6287](https://doi.org/10.1049/iet-pel.2018.6287).
- [21] Y. Jiang, Y. Yu, and X. Peng, "Online anomaly detection in DC/DC converters by statistical feature estimation using GPR and GA," *IEEE Trans. Power Electron.*, vol. 35, no. 10, pp. 10945–10957, Oct. 2020, doi: [10.1109/TPEL.2020.2981500](https://doi.org/10.1109/TPEL.2020.2981500).
- [22] Z. Xiao, "An instantaneously triggered short-circuit protection architecture for boost switching DC/DC converters," *IEEE Trans. Power Electron.*, vol. 33, no. 7, pp. 5677–5685, Jul. 2018, doi: [10.1109/TPEL.2017.2743170](https://doi.org/10.1109/TPEL.2017.2743170).
- [23] S. Yin et al., "Comparative Design of Gate Drivers with Short-Circuit Protection Scheme for MOSFET SiC and IGBT Si," *Energies*, vol. 12, no. 23, pp. 1–15, 2019, doi: [10.3390/en12234546](https://doi.org/10.3390/en12234546).
- [24] Report IEA-PVPS T13-19:2021, "Task 13 report the use of advanced algorithms in PV failure monitoring," *Int. Energy Agency*, 2021, ISBN 978-3-907281-07-9. [Online]. Available: [www.iea-pvps.org](http://www.iea-pvps.org)
- [25] A. Eskandari, J. Milimonfared, and M. Aghaei, "Fault detection and classification for photovoltaic systems based on hierarchical classification and machine learning technique," *IEEE Trans. Ind. Electron.*, vol. 68, no. 12, pp. 12750–12759, Dec. 2021, doi: [10.1109/TIE.2020.3047066](https://doi.org/10.1109/TIE.2020.3047066).
- [26] S. Bordihn, A. Fladung, J. Schlipf, and M. Köntges, "Machine learning based identification and classification of field-operation caused solar panel failures observed in electroluminescence images," *IEEE J. Photovolt.*, vol. 12, no. 3, pp. 827–832, May 2022, doi: [10.1109/JPHOTOV.2022.3150725](https://doi.org/10.1109/JPHOTOV.2022.3150725).
- [27] X. Cai and R. J. Wai, "Intelligent DC arc-fault detection of solar PV power generation system via optimized VMD-Based signal processing and PSO-SVM classifier," *IEEE J. Photovolt.*, vol. 12, no. 4, pp. 1058–1077, Jul. 2022, doi: [10.1109/JPHOTOV.2022.3166919](https://doi.org/10.1109/JPHOTOV.2022.3166919).
- [28] Y. Mahmoud, W. Xiao, and H. H. Zeineldin, "A simple approach to modeling and simulation of photovoltaic modules," *IEEE Trans. Sustain. Energy*, vol. 3, No 1, pp. 185–186, Jan. 2012, doi: [10.1109/TSTE.2011.2170776](https://doi.org/10.1109/TSTE.2011.2170776).
- [29] A. Gholami, M. Ameri, M. Zandi, R. G. Ghoachani, S. Pierfederici, and H. A. Kazem, "Step-by-Step guide to model photovoltaic panels: An up-to-date comparative review study," *IEEE J. Photovolt.*, vol. 12, no. 4, pp. 915–928, Jul. 2022, doi: [10.1109/JPHOTOV.2022.3169525](https://doi.org/10.1109/JPHOTOV.2022.3169525).
- [30] S. P. Boyd and L. Vandenberghe, *Introduction to Applied Linear Algebra: Vectors, Matrices, and Least Squares*. in Cambridge, U.K.: Cambridge Univ. Press, 2018.
- [31] P. E. Kakosimos, A. G. Kladas, and S. N. Manias, "Fast photovoltaic-system voltage or current-oriented MPPT employing a predictive digital current-controlled converter," *IEEE Trans. Ind. Electron.*, vol. 60, no. 12, pp. 5673–5685, Dec. 2013.
- [32] E. Bianconi et al., "A fast current-based MPPT technique employing sliding mode control," *IEEE Trans. Ind. Electron.*, vol. 60, no. 3, pp. 1168–1178, Mar. 2013.



**Diego Rivelino Espinoza-Trejo** (Senior Member IEEE) was born in San Luis Potosí, México. He received the B.S. degree in electronics engineering and the M.Sc. and Ph.D. degrees in electrical engineering from the Universidad Autónoma de San Luis Potosí, San Luis Potosí, México, in 2001, 2004, and 2008, respectively.

In 2009, he joined the Department of Mechatronics, Coordinación Académica Región Altiplano, Universidad Autónoma de San Luis Potosí. He is currently a Professor with the Universidad Autónoma de San Luis Potosí and a Researcher with the Consejo Nacional de Ciencia y Tecnología (CONACYT), Mexico City, México. His main research interests include modeling, control, and fault diagnosis techniques for grid-connected and autonomous photovoltaic systems.



**Luis Miguel Castro** graduated from the Instituto Tecnológico de Morelia in 2006, and received the Ph.D. degrees in electric power systems with Universidad Michoacana, Morelia, México, and Tampere University of Technology, Tampere, Finland, in 2013 and 2016, respectively.

He is currently a full-time Professor with the Department of Electrical Energy, Universidad Nacional Autónoma de México (UNAM), Mexico City, México. His research interests include the modeling, planning, and operation of ac/dc power systems with renewable energy sources.



**Ernesto Bárcenas** was born in San Luis Potosí, México. He received the B.S. degree in electronics engineering from the Universidad Autónoma de San Luis Potosí, San Luis Potosí, México, in 2000 and the M.Sc. and Ph.D. degrees in power electronics from the Centro Nacional de Investigación y Desarrollo Tecnológico, Cuernavaca, México, in 2002 and 2008, respectively.

Since 2010, he has been with the Coordinación Académica Región Altiplano, Universidad Autónoma de San Luis Potosí. His main research interests include power electronics for renewable energy applications, ac–dc conversion, and electric machine drives.



**José Pecina Sánchez** (Member, IEEE) was born in San Luis Potosí, México. He received the B.S. degree in electronics engineering, in 2010, and the M.S. degree in electrical engineering and the Ph.D. degree in electronics engineering from the Autonomous University of San Luis Potosí, San Luis Potosí, México, in 2012 and 2017, respectively.

He is currently a Professor and Academic Coordinator with the Department of Renewable Energy, Academic Coordination of the Altiplano-

Region Campus, Autonomous University of San Luis Potosí, San Luis Potosí, Mexico. His current research interests include modeling, control, and fault diagnosis of power conversion systems and electric machines; signal processing; and renewable energy systems technology.

Dr. Sánchez is a Member of the IEEE Power Electronics Society and belongs to the Mexican National System of Researchers.